nature communications

Article

https://doi.org/10.1038/s41467-025-68033-4

Viscoelastic hydrogel primed CAR-macrophage for pulmonary fibrosis treatment

Received: 27 January 2025

Accepted: 15 December 2025

Yan Zhang[1], Zhiqiang Liu[1], Wenyu Kong[1], Yanxiao Ao[1,2], Rui Zhang[1] & Yanan Du[1,3]

CAR-macrophage (CAR-M) therapy holds promise for the treatment of tumor and fibrotic diseases, yet genetic engineering remains the main efficacy-enhancing approach. Here we develop a non-genetic strategy using viscoelastic hydrogel to mechanically prime CAR-Ms. CAR-Ms exhibit potent phagocytosis of activated fibroblasts and collagen-degradation capacity, and hydrogel priming further enhances their cytotoxicity. Mechanistically, viscoelastic hydrogel priming reduces CAR-M membrane tension, which triggers membrane CAR to disassemble from clusters into dispersed monomers and dimers, leading to enhanced downstream signaling. In pulmonary fibrosis models, hydrogel-primed CAR-Ms demonstrate superior therapeutic outcomes, showing fibrosis reduction and microenvironment improvement. This study highlights CAR-M therapy's potential for pulmonary fibrosis treatment and offers a distinct approach to improve CAR-M efficacy by physical stimuli.

CAR-macrophage (CAR-M) therapy has been on the rise. Macrophages play a critical role in the innate immune system, where they clear apoptotic cells and pathogens[1,2]. Building on this, researchers have modified macrophages with chimeric antigen receptors (CARs) to enhance their ability to target and eradicate tumor cells specifically[3,4]. Additionally, given their tissue infiltration capacity, CAR-Ms have shown promising potential for solid tumors treatment[5,6]. Beyond being used to treat tumors, the application of CAR-M therapy can be extended to fibrotic disease treatments. Notably, a study employing anti-uPAR CAR-Ms in liver fibrosis treatment successfully alleviated fibrosis and improved the immune microenvironment[7]. These findings suggest that CAR-M therapy holds promise for treating parenchymal fibrotic diseases, as parenchymal fibrotic tissues also have compacted extracellular matrices and disordered immune microenvironments[8].

Pulmonary fibrosis is one of the most prevalent parenchymal fibrotic diseases[9,10]. Many risk factors, including smoking, chronic viral infections and environmental exposures, could induce pulmonary fibrosis. Pirfenidone and Nintedanib, the two FDA-approved drugs for pulmonary fibrosis, have shown effectiveness in suppressing fibrosis progression. However, their capacity to reverse or cure fibrosis is restricted[11–13]. As lung fibroblasts can be activated during pathogenesis, leading to excessive deposition of collagen fibers in the extracellular space of the alveoli[14], eliminating the activated fibroblasts provides the opportunity to disrupt this profibrotic positive feedback loop[15]. This eradication of activated fibroblasts can potentially be accomplished by specifically engineered CAR-Ms, where fibroblast activation protein (FAP) expressed by activated fibroblasts can serve as a target[16,17]. Despite this theoretical rationale, examples of using CAR-M therapy to treat pulmonary fibrosis, or even fibrotic diseases, are still rare. Moreover, to improve therapeutic outcomes, additional strategies should be employed to enhance the efficacy of CAR-M therapies.

Various methods have been applied to enhance CAR-M therapy efficacy: 1) Genetically modifying the CAR intracellular domain to contain the toll-like receptor 4 intracellular toll/IL-1R (TIR) can drive macrophages to polarize towards a proinflammatory M1 phenotype with stronger cytotoxicity[18]; 2) Directly edit macrophages, such as knocking out ACOD1, to polarize them toward pro-inflammatory state with stronger cytotoxicity, leading to better therapeutic outcomes[19,20];

---

[1]School of Biomedical Engineering, Tsinghua-Peking Joint Center for Life Sciences, Tsinghua University, Beijing, China. [2]State Key Laboratory of Membrane Biology-Membrane Structure and Artificial Intelligence Biology Branch, Beijing, China. [3]National Key Laboratory of Kidney Diseases, Beijing, China.
e-mail: duyanan@tsinghua.edu.cn

3) co-injecting CAR-Ms with CAR-T cells to augment therapeutic outcomes[21]. However, these methods have limitations, such as requiring extensive gene editing and being overly complex. Therefore, a non-gene-editing and more convenient method to enhance CAR-Ms performance is needed.

Harnessing the plasticity of macrophages offers an opportunity to enhance CAR-Ms functionality with greater convenience, especially when regulating CAR-Ms through physical stimuli[22,23]. Recent research has demonstrated that phenotypes of macrophages can be regulated by physical properties of the surrounding extracellular matrix (ECM) in vivo and the culture substrate in vitro. These mechanical properties include stiffness, viscoelasticity, and surface topography[24–27]. For instance, a gelatin scaffold with lower stiffness and smaller pore size can stimulate macrophages to polarize towards the pro-inflammatory phenotype[28]. Furthermore, viscoelasticity, a property of ECM that has recently been found crucial in regulating cellular behaviors, has been proven vital in regulating macrophage functionality. One recent study reported that macrophages cultured on a more viscous hydrogel substrate will exhibit higher phagocytosis level[29]. Similarly, another study demonstrated that viscoelastic substrates support stronger inflammatory responses of macrophages compared to elastic substrates[30]. These findings indicate that tuning the viscoelasticity of substrates offers an opportunity to improve CAR-Ms functionality by directly enhancing the cytotoxicity of the CAR-expressing macrophages. Furthermore, substrate viscoelasticity can also directly affect the CARs. CARs are expressed on the plasma membranes, making them inherently susceptible to alterations in membrane properties[31–33]. It has been reported that ECM physical properties, such as stiffness, can affect cellular membrane tension[34]. Moreover, the state and activation level of membrane proteins are also regulated by membrane tension[31,33,35–37]. Therefore, we hypothesize that the physical properties of the substrate can not only regulate macrophage phenotype but also affect the state of CAR and its related signaling directly.

In this study, we developed a distinct CAR-M system for alleviating pulmonary fibrosis. CAR-M was designed to target and eliminate activated fibroblasts in fibrotic lung, where Fap protein on their membrane was recognized as the target protein. Importantly, to enhance efficacy without gene editing, we primed CAR-Ms on designed hydrogel substrates with tunable viscoelasticity. Our findings demonstrated that, while maintaining the storage modulus of the hydrogel constant, CAR-Ms functionality was significantly improved after being seeded on the hydrogel with a specific loss modulus. Furthermore, we uncovered the mechanism underlying this priming effect. We found that viscoelastic hydrogel priming reduced CAR-Ms' membrane tension, leading to the disaggregation of CAR clusters, and elevated the ratios of CAR monomer and dimer. This dispersion phenomenon was further followed by the upregulation of CAR-related downstream signaling, which enhanced the cytotoxicity of CAR-Ms. Lastly, we verified the functionality of CAR-Ms in a murine pulmonary fibrosis model, where viscoelastic hydrogel-primed CAR-Ms also exhibited the strongest therapeutic effect. Our study not only introduces a distinct CAR-M therapy system for pulmonary fibrosis treatment, but also highlights that priming CAR-engineered cells with viscoelastic hydrogel could serve as an efficient and convenient method to improve their therapeutic effect.

Results

Construction and verification of a CAR-M system targeting activated fibroblasts

In this study, we constructed and verified a CAR-M system targeting activated pulmonary fibroblasts. Firstly, in order to identify the optimal anti-FAP single chain fragment variable (scFv), we collected two scFv sequences from existing literatures[38–40], and systematically compared their expression levels in both macrophage cell lines and primary macrophages. We found that two CAR constructs, FAP5 and MO36, exhibited high expression levels on human macrophage cell line (THP-1) (Fig. 1A, Supplementary Fig. 1A–C). Subsequently, we verified the functionality of FAP5 and MO36 constructs. We first test these two constructs on a conventional T cell model (Jurkat cell). We proved that CAR-Jurkat cells with FAP5 and MO36 constructs both exhibited elevated CD69 expression levels after a 12-hour co-culture with activated primary fibroblasts, suggesting that FAP5 and MO36 scFvs were indeed effective (Supplementary Fig. 2A). Furthermore, we evaluated the expression level of these CAR constructs on primary macrophages, as primary macrophages pose a greater challenge for lentivirus infection[3,41,42]. In this study, we employed murine bone marrow-derived macrophages (BMDMs) for primary-macrophage experiments. Our results revealed a higher proportion of CAR (FAP5)-positive BMDMs compared to CAR (MO36) after the same lentivirus infection process. This indicated the superior expression of CAR (FAP5) in BMDMs (Fig. 1B, Supplementary Fig. 3A, B). Therefore, it was selected for subsequent studies.

After identifying FAP5 construct as the optimal CAR construct, we conducted experiments to systematically verify its function on macrophages. In these experiments, we co-cultured CAR-Ms with target cells to assess their phagocytic and cytotoxic ability. Additionally, we investigate their collagen degradation capability by co-culturing them on a collagen hydrogel. First, we differentiated CAR-THP cells from monocytes into macrophages through treatment with 200 ng/mL PMA (Phorbol 12-Myristate 13-Acetate) for 48 hours. Successful differentiation was confirmed by the expression of CD14, CD68, and CD11b (Supplementary Fig. 4A). To assess the phagocytic ability of CAR-THP cells, we co-cultured them with FAP-expressing fibroblast cell line (3T3 cell). These two types of cells were respectively pre-labeled with DeepRed and Green cell trackers for visualization and tracking purposes. During the co-culture experiment, video recordings CAR-THP cells phagocytosing 3T3 cells were filmed (Supplementary Movie 1), and a time-series image sequence was obtained, which demonstrates the direct engulfment of target cells by CAR-THP cells (Fig. 1C). To quantitatively investigate the phagocytic ability of CAR-THP cells, all cells were extracted after co-culture and analyzed by flow cytometry. Results showed that the phagocytosis ratio of CAR-THP cells against 3T3 target cells was significantly higher than that of THP and Et-THP cells (Supplementary Fig. 5A, B). In this study, Et-THP refers to THP-1 cells with only truncated EGFR labeling. Additionally, to verify the specificity of CAR, an shRNA-mediated knockdown of FAP in 3T3 cells was performed to construct the FAP^{KD} 3T3 cell line (Supplementary Fig. 6A, B). Thereafter, we conducted a phagocytosis assay using 3T3 and FAP^{KD} 3T3 cells. The results revealed that CAR-THP cells exhibited a significantly higher phagocytosis rate against 3T3 cells compared to FAP^{KD} 3T3 cells (Fig. 1D), indicating that the CAR-Ms can specifically target cells that highly express FAP. Moreover, to assess the overall cytotoxic effect of CAR-Ms on target cells, we employed 3T3Aka (Akaluciferase-expressing 3T3) cells and quantified the bioluminescence intensity of the surviving 3T3Aka cells after a 24-hour co-culture. Results from this co-culture experiment showed that only CAR-THP cells exhibited significant cytotoxicity, while THP and Et-THP cells showed no evident cytotoxicity (Supplementary Fig. 7A). These results indicate that CAR-THP cells can effectively and specifically kill FAP high-expressing cells in vitro.

In addition to cytotoxicity verifications, we evaluated whether CAR-THP can directly degrade collagen upon activation. The collagen-degrading ability of CAR-THP was evaluated by seeding them onto TAMRA-labeled type I collagen hydrogel substrate with target cells (3T3 cells). When the collagen hydrogel was degraded, the labeled TAMRA was released, leading to a reduction in the TAMRA fluorescence in the remaining collagen hydrogel. Therefore, measuring the change of TAMRA fluorescence after the co-culture experiment would

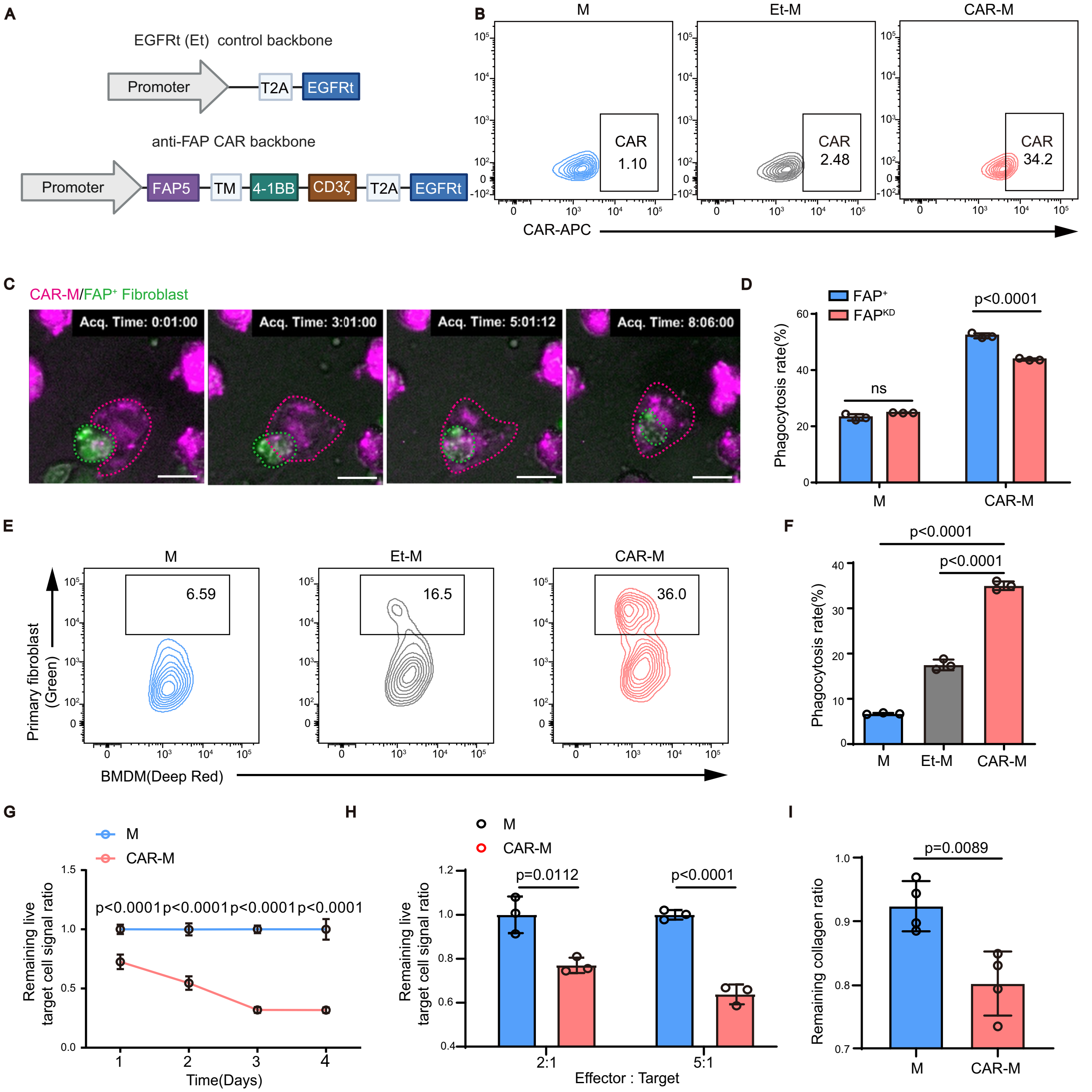

Fig. 1 | Construct and verify the CAR-M system targeting activated fibroblasts. **A** CAR construction with anti-FAP scFv and a control plasmid with only EGFRt (truncated EGFR). **B** Representative FACS plots of CAR expressed on lentivirus-infected BMDM. **C** Representative time-lapse pictures showing the process of CAR-THP (Pink) phagocytosing 3T3 cells (Green). Scale bar = 5 µm. **D** FACS-base analysis on the phagocytosis ratios of THP and CAR-THP phagocyting 3T3 and FAP^{KD} 3T3 cells. *n* = 3 independent experiments. Statistical significance was calculated with two-way ANOVA analysis and is presented as mean ± s.d. Exact *P* values are labeled. **E** Representative FACS plot of BMDMs, Et-BMDMs and CAR-BMDMs (DeepRed) phagocytosed with pFs (Green). **F** FACS-based analysis on the phagocytosis ratios of BMDMs, Et-BMDMs and CAR-BMDMs phagocyting pFs. *n* = 3 biological replicates. Statistical significance was calculated with one-way ANOVA analysis with multiple comparisons and is presented as mean ± s.d. Exact *P* values are labeled. **G** Bioluminescence from the survived targeted 3T3Aka cells at a 2:1 E:T ratio after 1 Day, 2 Days,3 Days and 4 Days. Normalize to macrophage group. *n* = 3 independent experiments. Statistical significance was calculated with two-way ANOVA analysis and is presented as mean ± s.d. **H** Bioluminescence from the survived targeted 3T3Aka cells at a 2:1 and 5:1 E:T ratio for 1 Day. Normalize to macrophage group. *n* = 3 independent experiments. Statistical significance was calculated with two-way ANOVA analysis and is presented as mean ± s.d. **I** Fluorescence-based analysis on the remaining collagen ratios of substrate where BMDMs and CAR-BMDMs were co-cultured with 3T3 cells. *n* = 4 independent experiments. Significance was calculated with unpaired two-tailed *t* test and is presented as mean ± s.d.

directly indicate the collagen degradation of activated CAR-THP. Results showed that CAR-THP cells degraded a significantly larger amount of collagen compared with THP and Et-THP cells when stimulated by 3T3 cells (Supplementary Fig. 7B). These results demonstrated that the degradative capacity of macrophages can be enhanced through CAR activation. In addition, to further verify the versatility of our CAR system on macrophages, we utilized a mouse macrophage cell line, RAW264.7 (Supplementary Fig. 8A), to conduct both killing assay and the collagen degradation assay. As anticipated, CAR-RAW cells demonstrated stronger cytotoxicity and collagen degradation ability than RAW cells (Supplementary Fig. 8B, C). These results verified that the CAR-M system we established can effectively eliminate target cells and degrade surrounding collagen fibers in vitro.

Building on the aforementioned data, we employed BMDMs to evaluate the effectiveness of our CAR system on primary cells, paving the way for the following in vivo experiments. The phagocytic capability of CAR-BMDM was first evaluated. We proved that the phagocytosis ratio of CAR-BMDMs against TGF-β-stimulated primary lung fibroblasts was significantly higher than that of non-engineered BMDMs (Fig. 1E, F). Here, TGF-β-stimulation is implemented to activate primary fibroblasts to upregulate FAP, resembling their status in fibrotic lungs (Supplementary Fig. 9A–C). Moreover, by extending coculturing time as well as adjusting E:T ratio (Effector: Target), we found that CAR-BMDMs eradicated 3T3 target cells in both dose- and time-dependent manners (Fig. 1G, H). This result proved the efficacy and specificity of the CAR-BMDMs. Furthermore, we evaluated the capability of CAR-BMDM to directly degrade collagen. We conducted the collagen degradation assay and found that CAR-BMDMs demonstrated superior degradation performance compared to BMDMs after being activated by target cells (Fig. 1I). In sum, these results demonstrated that the CAR system we have built significantly enhanced the phagocytic capability and cytotoxicity against activated primary fibroblasts. Additionally, the direct collagen degradation capability of CAR-BMDMs is also significantly promoted compared to non-engineered BMDMs after being activated by target cells. Collectively, these results indicated the effectiveness of our CAR system on primary macrophages, laying down the foundation for their therapeutic efficacy in vivo.

Viscoelastic hydrogel substrate primed CAR-Ms with stronger functionality in vitro

To further enhance the efficacy of CAR-Ms, we seeded them onto a viscoelastic substrate to prime them with physical stimuli (Fig. 2A, B). A hydrogel system with tunable viscoelasticity was constructed based on previous studies[43–45]. These viscoelastic hydrogels are composed of gelatin and oxidized alginate. By altering the oxidation degree of alginate while maintaining the mass ratio of gelatin to alginate, loss modulus of hydrogels can be tuned while their storage modulus remained constant (Fig. 2B). In this hydrogel system, increasing the oxidation degree of alginate will decrease the ratio of ionic bonds to imine bonds, resulting in decreased loss modulus and slower stress relaxation properties (Supplementary Fig. 10). To confirm the viscoelasticity of these hydrogels. We measured their storage modulus (G′) and the loss modulus (G”), as well as their relaxation rates. We proved that while the storage modulus of hydrogel was kept relatively constant at ~1.3 KPa (Fig. 2C), the loss modulus showed a gradient decrease along the increment of oxidation degree of alginate (Fig. 2D). Correspondingly, hydrogels with lower oxidation degrees exhibited faster stress relaxation rates (Fig. 2E). Together, these data showed that our hydrogel system possess tunable viscoelasticity, which paved the way for following experiments investigating effects of hydrogel viscoelasticity on CAR-Ms functionalities.

To evaluate the effect of hydrogel viscoelasticity on CAR-Ms' function, a killing assay was first conducted, which compared CAR-Ms with hydrogel-primed CAR-Ms (Gel-CAR-Ms), as well as compared with Il4- and LPS-stimulated CAR-Ms. Notably, hydrogel with 50% alginate oxidation degree exhibited the most significant enhancement of CAR-Ms cytotoxicity, outperforming untreated cells and those CAR-Ms stimulated by IL-4 or LPS. Importantly, this priming effect of viscoelastic hydrogel was verified in both macrophage cell lines and primary cells (BMDMs), respectively (Fig. 2F, G). Consequently, the hydrogel produced with 50% oxidized alginate was selected for all subsequent experiments. In order to further validate the effect of hydrogel priming, we co-cultured Gel-CAR-M (BMDMs) with activated primary lung fibroblasts (Supplementary Fig. 11A). The results showed that Gel-CAR-Ms exhibited enhanced cytotoxicity even against primary target cells, confirming the robustness of the hydrogel priming effect. Notably, the hydrogel-induced enhancement in cytotoxicity remained evident throughout the 48-hour co-culture period (Supplementary Fig. 11B), indicating that the priming effect is durable. To further investigate the impact of hydrogel priming on CAR-Ms recognition and activation against target cells, key phosphorylated proteins involved in the CAR-related downstream signaling pathway were evaluated with immunofluorescence (Fig. 2H). After a 4-hour co-culture, Gel-CAR-Ms exhibited upregulated p-SYK, p-ERK1/2 and p-JNK expression compared to CAR-Ms, indicating their higher cytotoxicity (Fig. 2H, Supplementary Fig. 11C). To further investigate the transcriptomic differences between CAR-Ms and Gel-CAR-Ms, we performed bulk RNA sequencing. Differentially expressed genes between the two groups were significantly enriched in the MAPK signaling pathway (Fig. 2I). This finding is consistent with the staining results. Furthermore, volcano plot analysis revealed that hydrogel priming upregulated several immune regulatory and ECM remodeling-related genes in CAR-Ms[46,47], including *Ccl5*, *Cxcl10*, and *Mmp13* (Supplementary Fig. 12A). We also visualized representative genes using a heatmap categorized by functional annotations (Supplementary Fig. 12B). Results showed that Gel-CAR-Ms displayed downregulation of pro-fibrotic genes (*Col1a1*, *Fn1*, *Tgfb1*), indicating anti-fibrotic potential. The transcriptional-level change of these genes suggests that Gel-CAR-Ms may exhibit promoted therapeutic effects in pulmonary fibrosis through enhanced immunomodulation and matrix remodeling function.

Further, we investigated whether this hydrogel priming effect can be extended to other CAR-engineered cells. We discovered that cytotoxicity of anti-CD19 CAR-T cells was also significantly enhanced after being primed by viscoelastic hydrogels (Supplementary Fig. 13A). Moreover, we verified that viscoelastic hydrogel-primed CAR-T (Gel-CAR-T) cells indeed showed upregulation of cytotoxicity-related factors, such as *IL2* and *IFN-γ* (Supplementary Fig. 13B).

Our results demonstrated that a hydrogel with suitable viscoelasticity can significantly enhance CAR-M functionalities. Importantly, we showed that this priming effect can be extended to CAR-T cells, suggesting its general significance in enhancing the performance of CAR-engineered cells.

Viscoelastic hydrogel promotes CAR-M functionality by redistributing membrane CARs

In this section, we explored the mechanism underlying the priming effect of viscoelastic hydrogel on CAR-Ms from the perspective of mechanobiology. CAR is a membrane protein, suggesting its expression and functional performance are intricately connected to the cell membrane properties[31,48,49]. Therefore, stimuli, including physical stimuli brought by our viscoelastic hydrogel, can affect CAR by affecting the cell membrane. Here, we focused on the membrane tension of CAR-Ms as it may be directly influenced by the mechanical properties of the ECM[34,50].

First, we investigated how viscoelastic hydrogel affected the plasma membrane tension of CAR-Ms. We evaluated the cell membrane tension using the Flipper TR fluorescent probe, which can insert into plasma membranes and indicate membrane tension through fluorescence-lifetime change[51]. Our findings demonstrated a significant reduction in cell membrane tension in Gel-CAR-Ms compared to CAR-Ms (Fig. 3A, B). Subsequently, we tracked the change of CAR distribution on the membrane by conjugating them with an mCherry fluorescent protein on the C-terminus. Confocal microscopy was employed to monitor the change in CAR distribution, revealing a more dispersed distribution pattern of CAR on hydrogel-primed cells as CAR clusters largely disaggregated (Fig. 3C, D). Moreover, to conduct a more precise examination of CAR distribution, total internal reflection fluorescence (TIRF) microscopy was utilized to observe membrane CAR. Our result showed that CAR clusters on CAR-Ms membrane were

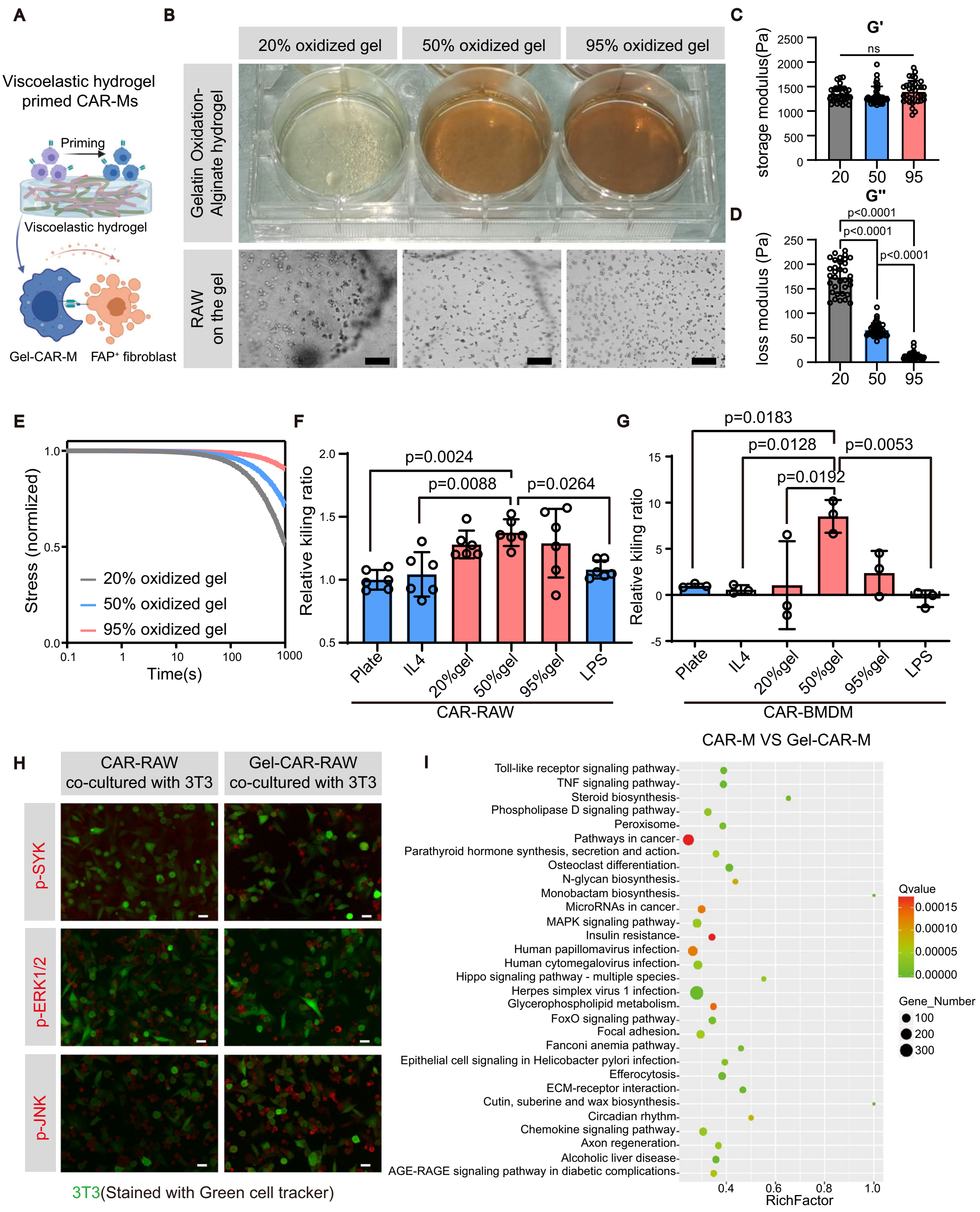

diminished after hydrogel priming (Fig. 3E, F). These findings indicated that hydrogel priming decreased the cell membrane tension of CAR-Ms, as well as reduced the aggregation of CAR on the cell membrane. We hypothesized that reduced cell membrane tension can lead to CAR redistribution, thus enhancing CAR self-activation. This could result in a highly prepared state for CAR-Ms and enable a more vigorous response to stimulation from target cells (Fig. 3G).

To investigate how the change in CAR distribution, caused by viscoelastic hydrogel, affected CAR-Ms functionality, we conducted a non-reducing western blot experiment on CAR-Ms and Gel-CAR-Ms. A significant increase in the proportions of CAR monomers and dimers was observed in Gel-CAR-Ms (Fig. 3H–J). In addition, we characterized the change in ERK1/2 and p-ERK1/2 levels in CAR-Ms without target cells. As a result, a two-fold upregulation of (p-ERK1/2)/(ERK1/2) ratio

Fig. 2 | Viscoelastic hydrogel substrate endows CAR-Ms with enhanced functionality. A Schematic of hydrogel primed CAR-Ms eradicating target cell. **B** Appearance of Gelatin Oxidized-Alginate hydrogel with different oxidation degrees in a six-well plate and RAW264.7 being seeded on these hydrogels. Here, 20% oxidized gel, 50% oxidized gel, and 95% oxidized gel refer to hydrogels produced with 20%, 50%, and 95% oxidized alginate, respectively. Scale bar = 100 μm. **C** Storage modulus of hydrogel with different oxidation degree. *n* (20% and 50%) = 36, *n* (95%) = 34 technical replicates from three biological experiments. **D** Loss modulus of hydrogel with different oxidation degrees. *n* (20%) = 34, *n* (50% and 95%) = 36 technical replicates from three biological experiments. **E** Normalized stress relaxation curves of hydrogel with different oxidation degree. **F** Relative killing ratio of hydrogel primed CAR-RAW, Il4 stimulated CAR-RAW, and LPS stimulated CAR-RAW toward target 3T3Aka. Here, 20% gel, 50% gel, and 95% gel refer to hydrogels produced with 20%, 50%, and 95% oxidized alginate, respectively. *n* = 6. Normalize to the macrophage group. **G** Relative killing ratio of hydrogel primed CAR-BMDM, Il4 stimulated CAR-BMDM, and LPS stimulated CAR-BMDM toward target 3T3Aka. Here, 20% gel, 50% gel, and 95% gel refer to hydrogels produced with 20%, 50%, and 95% oxidized alginate, respectively. Normalize to the macrophage group. *n* = 3 independent experiments. **H** Immunostaining for p-SYK, p-ERK1/2, and p-JNK in CAR-RAW and Gel-CAR-RAW cells. NIH3T3 cells were labeled with CellTracker Green. Scale bar was 10 μm. **I** KEGG pathway enrichment analysis (CAR-M vs Gel-CAR-M, *n* = 3 per group). Bubble plot showing significantly enriched pathways based on differentially expressed genes. Statistical significance was calculated with one-way ANOVA analysis with multiple comparisons and is presented as mean ± s.d (**C**, **D**, **F** and **G**). Exact *P* values are labeled. **A** was created with BioRender. Lab, D. (2025) https://BioRender.com/26mqfo7.

was observed in Gel-CAR-Ms. These results indicated that viscoelastic hydrogel will significantly promote disaggregation of CAR and the self-activation level of CAR downstream pathway (Fig. 3K, L), which supports our hypothesis that hydrogel priming reduces cell membrane tension, leading to a preference for CAR to exist as monomers or dimers on the membrane, thereby amplifying downstream CAR signaling.

To further verify our conclusion, we characterized the change of CAR distribution specifically on plasma membranes with a single-molecule photobleaching assay (Fig. 3M). We discovered that the ratio of CAR monomers (Fig. 3N) and dimers (Fig. 3O) on CAR-Ms membranes was significantly elevated.

To further confirm our hypothesis, we used N-(3-Oxododecanoyl) (3oc) as a substitute for viscoelastic hydrogel priming to reduce the membrane tension of CAR-Ms (Fig. 3P). 3oc is a commonly used small molecule to reduce cell membrane tension[52]. Our results demonstrated a marked reduction in CAR clustering following the treatment of 3oc (Fig. 3Q, R). This data supported our hypothesis that the reduction of cell membrane tension will lead to the dispersion of CARs, which can be reflected from the decrease of CAR cluster number verified by TIRF microscopy (Fig. 3Q, R). Furthermore, we discovered that the dispersion of CAR caused by 3oc treatment also significantly elevated the killing ratio of CAR-Ms, which emphasized that reducing membrane tension could lead to CAR dispersion and enhanced CAR-Ms functionality (Fig. 3S).

Based on these findings, we demonstrated that viscoelastic hydrogel can reduce CAR-Ms membrane tension and lead to the dispersion of membrane CARs. This dispersion of CAR was found to correlate with the elevation of self-activation of CAR, which prepared CAR-Ms to rigorously respond to target cells.

Gel-CAR-Ms possess enhanced therapeutic effects in pulmonary fibrosis treatment

To evaluate the therapeutic effect of CAR-Ms and Gel-CAR-Ms in treating lung fibrosis, we administered these cells into mice with pulmonary fibrosis, followed by monitoring therapeutic outcomes.

First, we established a pulmonary fibrosis mouse model induced by bleomycin. To validate this model, we performed micro-CT imaging analysis and hydroxyproline (HYP) content analysis on model mice. Results showed a significant increase in the volume of fibrotic tissue in the lungs of bleomycin-induced mice, along with an evident elevation in lung tissue HYP content (Fig. 4A, B). These results confirmed successful pulmonary fibrosis model establishment. Importantly, we employed immunofluorescence staining to verify the elevation of FAP and α-SMA in fibrotic lung tissue sections, which indicated an increased population of activated fibroblasts (Fig. 4A). These results not only verified the successful establishment of pulmonary fibrosis mouse model, but also supported our rationale on using FAP as targeting protein.

The CAR-M therapy was conducted by administering cells into model mice. In this study, we administered CAR-Ms and Gel-CAR-Ms into mice with pulmonary fibrosis through the tail vein on days 7 and 14 after bleomycin induction, with phosphate-buffered saline (PBS), and macrophage (M) groups as control groups. On day 21, we collected samples by sacrificing the mice (Fig. 4C). Throughout the study, we continuously monitored the body weight of the mice (Fig. 4D). By the time of sample collection, the most notable increase in body weight was observed in the Gel-CAR-M group. In addition, HYP concentration of mice's lung in Gel-CAR-M group displayed the most markedly decrease (Fig. 4E). These results suggested that Gel-CAR-M treatment alleviated pulmonary fibrosis efficiently.

To further assess the therapeutic effects of CAR-Ms, we conducted Masson’s trichrome, hematoxylin-eosin (HE) and Sirius Red staining on lung sections from CAR-M and Gel-CAR-M treated mice (Fig. 4F). Both Masson’s Trichrome and Sirius Red staining revealed a significant reduction in pulmonary fibrosis in CAR-M and Gel-CAR-M treated groups, with Gel-CAR-Ms showing superior therapeutic effects (Fig. 4G–I). Additionally, HE staining and Ashcroft scoring showed thinning of the interstitial space and restoration of the normal alveoli structure in CAR-M and Gel-CAR-M treated mice, especially Gel-CAR-M group (Fig. 4F, H). Collectively, the section staining images and statistical analyses suggested that both CAR-M and Gel-CAR-M treatments improve lung fibrosis and tissue architecture, with Gel-CAR-Ms demonstrating superior therapeutic effects.

Following this, in order to evaluate the clearance of activated fibroblasts in the lungs after treatment, immunofluorescence staining of FAP was performed (Fig. 5A). The results demonstrated the effective clearance of activated fibroblasts by both CAR-Ms and Gel-CAR-Ms from the lowered FAP signal in lung sections, with Gel-CAR-Ms exhibiting a more pronounced clearance effect (Fig. 5B). Importantly, we also verified the localization of CAR-Ms in the treated lungs. Tracking of injected CAR-Ms was accomplished utilizing CD45.1-positive macrophages and CD45.2-positive mice in the experiment. The identification of CD45.1-positive cells in the interstitial spaces of the lung tissue suggested that the injected cells are capable of persisting within the lung tissue throughout the treatment process (Fig. 5C). Following this, we further evaluated the biodistribution and retention of injected Gel-CAR-Ms using DiR fluorescence labeling. Whole-organ fluorescence imaging was conducted on days 1, 7, 14, and 21 after administration to assess the in vivo localization and persistence of the injected cells. These results revealed that Gel-CAR-Ms primarily accumulated in the lungs, liver and spleen (Supplementary Fig. 14A). Quantitative analysis of fluorescence intensity showed a rapid decline in DiR signal in the lungs during the first 7 days, followed by a slight decrease thereafter, indicating sustained retention of CAR-Ms in the lung tissue beyond day 7. (Supplementary Fig. 14B).

Additionally, to investigate the changes in the immune microenvironment of the mouse lungs post-treatment, we utilized qPCR to assess the gene expression of collagen, cytokines, chemokines, and matrix metalloproteinases (MMPs) at the tissue level (Fig. 5D). As anticipated, the heatmap generated from qPCR results revealed elevated expression levels of inflammatory and chemotactic factors in

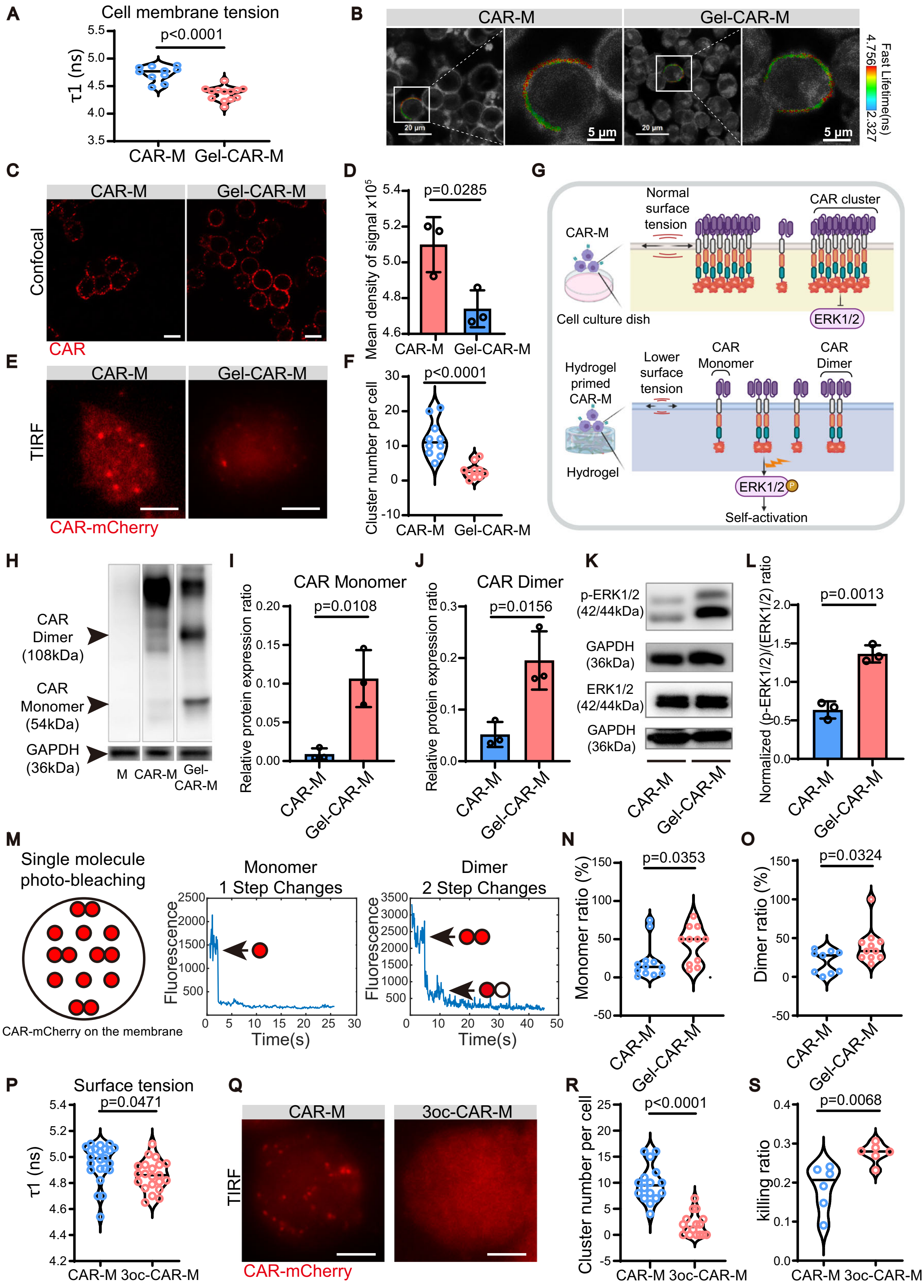

PBS-treated lungs. Moreover, we discovered that although non-engineered macrophages lowered the expression level of inflammatory and chemotactic factors in the lung, they upregulated the collagen-related genes, which may lead to their unsatisfactory therapeutic effect. Additionally, CAR-M treated fibrotic lungs displayed an upregulation of interleukin factors, which is unfavorable for fibrosis alleviation. Importantly, we discovered that Gel-CAR-Ms decreased the overall expression of all collagen, cytokines, and chemokines related genes. Specifically, in the Gel-CAR-M group, the expression of fibrosis-related genes *Acta2* and *Col2a1* was significantly downregulated (Fig. 5E–G), as well as the expression of chemokines (Ccl1, Ccl2) and cytokines (Il6) (Fig. 5H–J). This phenomenon suggested that Gel-CAR-

Fig. 3 | Decrease of cell membrane tension leads to membrane CAR redistribution with upregulation of p-ERK. A Cell membrane tension parameter of CAR-Ms and Gel-CAR-Ms. *n* (CAR-M) = 10, *n* (Gel-CAR-M) = 13 cells from three independent experiments. **B** Representative images showing the measurement of the fluorescence lifetime of the Flipper TR fluorescent probe on the cell membrane. Left: Scale bar = 20 μm. Right: scale bar = 5 μm. **C** Representative confocal image of CAR-Ms and Gel-CAR-Ms. CAR expression was visualized using an Alexa Fluor 649-conjugated secondary antibody (shown in red). **D** Mean fluorescence intensity per unit fluorescence area. *n* = 3 three independent views. **E** Representative TIRF images of CAR-Ms and Gel-CAR-Ms. **F** Quantified CAR cluster per cell. *n* = 10 from three independent experiments. **G** Hypothesized schematic of CAR protein distribution pattern changes before and after hydrogel priming. **H** Representative western blotting of CAR dimer and CAR monomer in Ms, CAR-Ms and Gel-CAR-Ms. **I** Relative CAR protein monomer expression ratio in CAR-Ms and Gel-CAR-Ms. *n* = 3 independent experiments. **J** Relative CAR protein dimer expression ratio in CAR-Ms and Gel-CAR-Ms. *n* = 3 independent experiments. **K** Representative western blotting of p-ERK1/2 and ERK1/2 in CAR-Ms and Gel-CAR-Ms. **L** Normalized relative (p-ERK1/2)/(ERK1/2) ratio in CAR-Ms and Gel-CAR-Ms. Normalize to CAR-M group. *n* = 3. **M** Diagram of CAR protein detection by single-molecule photobleaching. **N**, **O** CAR protein monomer ratio and dimer ratio on CAR-Ms and Gel-CAR-Ms. *n* = 10 from three independent experiments. **P** Cell membrane tension parameter of CAR-Ms and 3oc-CAR-Ms by Flipper TR fluorescent probe. *n* (CAR-M) = 23, *n* (3oc-CAR-M) = 21 from three independent experiments. **Q** Representative TIRF image of CAR-Ms and Gel-CAR-Ms. **R** Quantified CAR cluster number on CAR-Ms and 3oc-CAR-Ms. *n* = 16 from three independent experiments. **S** Killing ratio of CAR-Ms and 3oc-CAR-Ms against 3T3Aka cells. *n* = 6 independent experiments. Statistical significance was calculated with unpaired two-tailed *t* test and is presented as mean ± s.d. (**A**, **D**, **F**, **I**, **J**, **L**, **N**, **O**, **P**, **R**, and **S**). Exact *P* values are labeled. Scale bar of (**C**, **E**, and **Q**) was 5 μm. **G** was created with BioRender. Lab, D. (2025) https://biorender.com/kfxx0k2.

Ms can restore the immune microenvironment of lungs, reducing inflammation and collagen deposition levels, resulting in the enhanced therapeutic effect compared to macrophages and CAR-Ms.

To assess the long-term safety of the Gel-CAR-M therapy, we conducted comprehensive safety evaluations over a 12-week period following treatment. Complete blood count analyses were performed at weeks 4 and 8 post-treatment in healthy, fibrotic, and Gel-CAR-M treated mice (Supplementary Fig. 15A). At 4 weeks, most hematological parameters, including white blood cells, red blood cells, hemoglobin, neutrophils and lymphocytes, had reached comparable levels across groups, with the exception of platelet counts. By 8 weeks, all complete blood count parameters exhibited no significant differences among the three groups, indicating hematological recovery following treatment. Additionally, histological examination of major organs, including the heart, liver, spleen, kidney, and femur, was performed at week 12 via H&E staining (Supplementary Fig. 15B). All groups displayed normal tissue architecture without signs of inflammation, fibrosis, or cellular damage, suggesting that Gel-CAR-M therapy does not induce off-target organ toxicity. Further, serum biochemical indices were also evaluated at 12 weeks to monitor hepatic and renal function, as well as potential autoimmune responses (Supplementary Fig. 15C). No significant differences were observed in levels of liver function markers including alanine aminotransferase (ALT), aspartate aminotransferase (AST), and alkaline phosphatase (ALP), or renal function markers including blood urea nitrogen (UREA) and uric acid (UA) among the groups. Furthermore, serum anti-nuclear antibody (ANA) levels remained comparable across all groups, indicating that Gel-CAR-M treatment did not trigger systemic autoimmunity. Collectively, these results confirm the long-term safety of Gel-CAR-M therapy at the hematological, histological, and biochemical levels.

Discussion

This study established a distinct CAR-M-based anti-pulmonary fibrosis therapy. Moreover, this study improved the therapeutic effect of CAR-Ms by treating them with a viscoelastic hydrogel substrate. We discovered that viscoelastic hydrogel can redistribute membrane CAR into a more dispersed pattern by lowering the cell membrane tension. This redistribution of CAR is followed by the upregulation of CAR-related downstream pathway, thereby preparing CAR-Ms into a more ready state to respond to target cells (Fig. 6).

Pulmonary fibrosis is a prevalent disease. The key cells that contribute to fibrosis progression are activated fibroblasts in the lungs. In our study, we used CAR-Ms to precisely target and eliminate activated fibroblasts. Macrophages, in addition to their cytotoxic effects, possess collagen-degradative and immunoregulatory capabilities that hold promising therapeutic potential for fibrotic disease treatment. A study on CAR-M therapy for liver fibrosis revealed that CAR-Ms can modulate the local tissue microenvironment, resulting in the regression of fibrosis[7]. Similarly, our research revealed that Gel-CAR-Ms therapy can modulate the immune microenvironment in fibrotic lungs, leading to a downregulation of inflammation-related genes (Fig. 5D). However, in our research, we have advanced by employing a fluorescent collagen hydrogel degradation assay to quantitatively characterize the degradation capacity of CAR-Ms in vitro. And our results demonstrated that CAR-Ms can directly degrade surrounding collagen fibers. This implied that CAR-Ms may have a direct degradation function in vivo as well. Despite these findings, additional details, such as the MMP profile and the dominant MMPs secreted by CAR-Ms, require further investigation. In addition, there has been a study that constructed MMP-secreting CAR-M containing transmembrane and intracellular regions of the mouse CD147 molecule[53]. The expression of multiple MMPs was upregulated upon CAR-Ms stimulation. Based on this study and our work, we could potentially create more effective CAR-Ms for fibrotic disease therapy by incorporating domains that enhance degradative functions into CAR.

Selecting the appropriate target is crucial in CAR-M therapy for treating fibrotic diseases. In addition to FAP, platelet-derived growth factor receptor (PDGFR) emerges as another significant target in fibrosis tissue[54]. PDGFR is essential for mesenchymal cell development and plays a pivotal role in fibroblast activities, particularly involved in tissue homeostasis and regeneration. Activation of PDGFRβ signaling stimulates fibroblasts, promoting the production of ECM proteins essential for tissue restoration[55]. The PDGF/PDGFR signaling pathway is implicated in various fibrosis disease processes, including cardiac fibrosis, liver fibrosis and renal fibrosis[56]. In cancer, PDGFRβ expression is also upregulated in cancer-associated fibroblasts (CAFs)[54]. Previous studies have developed CAR-T cells targeting PDGFRβ for the treatment of rhabdomyosarcoma, showing improved tumor regression and survival in subcutaneous xenograft models[57]. Therefore, PDGFRβ could also be a viable target for CAR-M therapy in pulmonary fibrosis. Furthermore, combining diverse CARs and employing various CAR designs[58,59] could serve as potent strategies to augment the efficacy of CAR-M therapy.

Currently, there is a gradual increase in research on CAR-M. Researchers are actively enhancing CAR-Ms for improved therapeutic efficacy. One study incorporated TIR into the CAR intracellular domain to modulate CAR-M phenotype and enhance its cytotoxicity[18]. Another study knocked out specific genes, thereby augmenting CAR-M's phagocytic capacity and anti-tumor activity[19]. Compared to previous studies, we prime CAR-Ms on the specific viscoelastic hydrogel instead of gene editing. This method significantly improved CAR-Ms cytotoxicity with high convenience. Thus, our study offered a distinct non-gene-editing method to augment CAR-Ms' effectiveness. Furthermore, according to the gene expression heatmap of the lungs, Gel-CAR-Ms did not trigger severe side effects like cytokine release syndrome. In addition to evaluating therapeutic efficacy, we also conducted a comprehensive long-term safety assessment 12 weeks after cell therapy. Serum biochemical indices, including liver function markers and

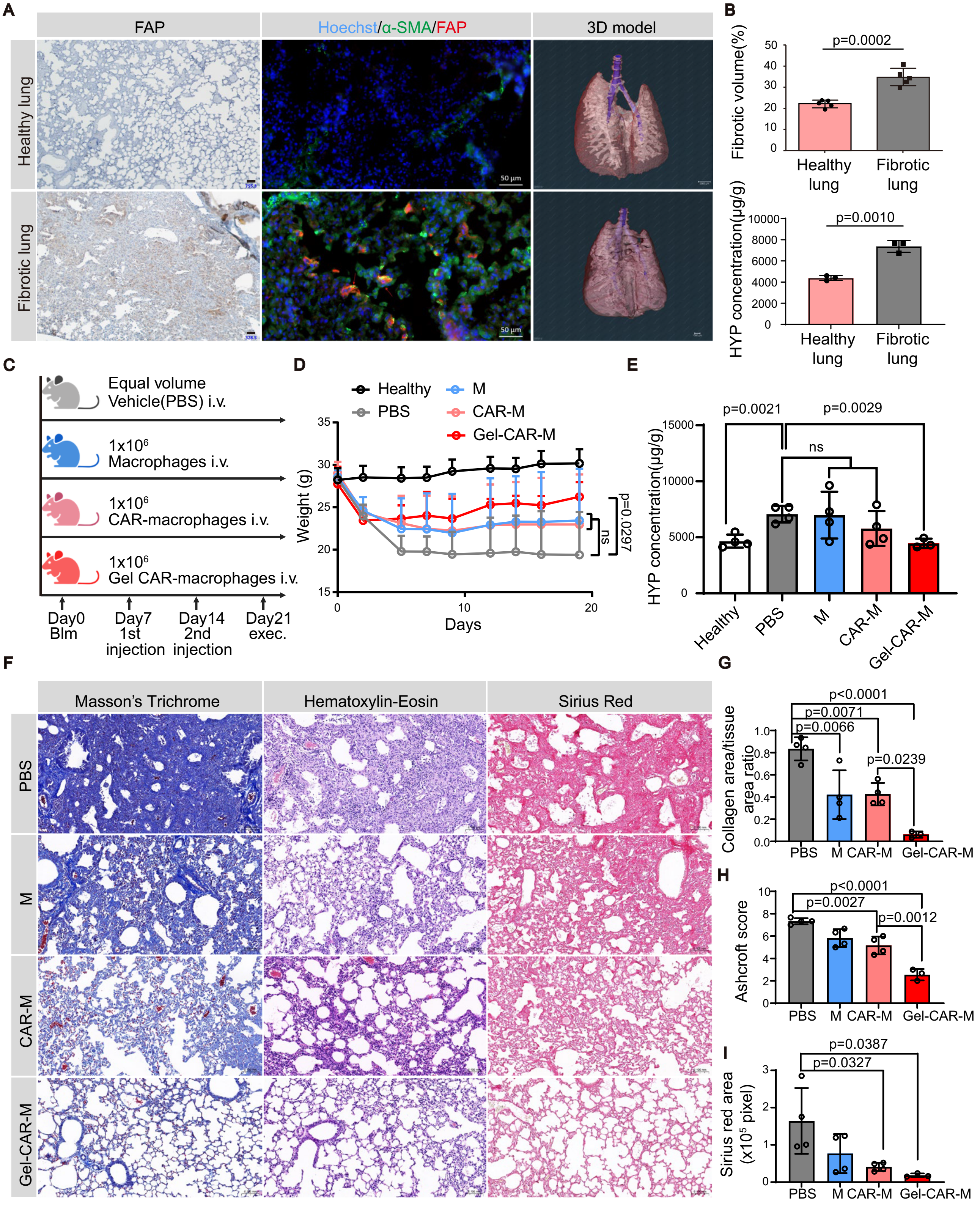

kidney function markers, returned to normal ranges across all groups (Supplementary Fig. 15). Furthermore, serum anti-nuclear antibody levels remained unchanged, indicating that Gel-CAR-M treatment did not induce autoimmune responses. Histological analyses of major organs, including the heart, liver, spleen, kidneys, and bones, revealed no signs of inflammation or tissue damage, with all organs maintaining normal architecture. These results collectively demonstrate that Gel-CAR-M therapy is not only effective but also well-tolerated, exhibiting no systemic toxicity or immune-related adverse effects over extended observation periods.

Research on the influence of cell fate by substrate mechanical memory and dosing has been ongoing. It has been observed that a supraphysiological stiff substrate, TCP, can induce sustained activation of the YAP signal in hMSCs[60]. When cells are cultured on hydrogels with increased Young's modulus, the YAP signal exhibits a dose-dependent activation related to the stiffness of the hydrogel. This

Fig. 4 | Hydrogel priming improved the therapeutic effect of CAR-M on murine pulmonary fibrosis model. A FAP (Red) immunostaining with α-SMA (Green) and micro-CT image 3D reconstruction of the mouse healthy lung and fibrotic lung. Cell nuclei are stained with Hoechst (blue). Scale bar was 50 μm. **B** Statistic of micro-CT fibrotic tissue volume ratio (*n* = 5 mice) and HYP concentration in healthy lung and fibrotic lung (*n* = 3 mice). Statistical significance was calculated with an unpaired two-tailed *t* test and is presented as mean ± s.d. **C** C57BL/6 mice were intratracheal injected with bleomycin and treated with PBS, M, CAR-M and Gel-CAR-M through the tail vein twice 7 d later. **D** Weight change of mice with different treatments. *n* (Healthy) = 6, *n* (PBS) = 4, *n* (M) = 5, *n* (CAR-M) = 5, *n* (Gel-CAR-M) = 3 mice. Statistical significance was calculated with two-way ANOVA analysis with multiple comparisons and is presented as mean ± s.d. **E** HYP concentration of lung. *n* (Healthy) = 4, *n* (PBS) = 4, *n* (M) = 4, *n* (CAR-M) = 4, *n* (Gel-CAR-M) = 3 mice. Among the five groups, a significant difference was observed by one-way ANOVA ($P < 0.05$). Subsequently, an unpaired two-tailed *t* test was performed to specifically compare the significance of two groups. Results are presented as mean ± s.d. **F** Representative Masson's Trichrome, Hematoxylin–Eosin and Sirius Red staining picture of lung tissue with different treatments. Scale bar was 100 μm. **G** Statistic of collagen tissue area ratio in total tissue area by Masson's Trichrome staining pictures. **H** Ashcroft score of lung tissue by Hematoxylin-Eosin staining pictures. **I** Collagen fiber area of lung tissue by Sirius Red staining pictures. **G**–**I** average of three views of one sample was calculated and taken into statistics. *n* (PBS) = 4, *n* (M) = 4, *n* (CAR-M) = 4, *n* (Gel-CAR-M) = 3 mice. Statistical significance was calculated with one-way ANOVA and is presented as mean ± s.d (**G**–**I**). Exact *P* values are labeled. **C** was created with BioRender. Lab, D. (2025) https://BioRender.com/q3zl6iz.

mechanically induced activation gradually transitions to irreversible activation with prolonged culture time. Further investigations suggest that the key factors behind the emergence of mechanical memory is epigenetic regulation[61–63]. Nuclear deformation and actomyosin contractility can lead to persistent epigenetic changes, such as acetylation and methylation of histone tails, as well as DNA methylation in promoter regions. These changes affect chromatin organization, condensation, and accessibility of transcription factors. In our study, Gel-CAR-Ms exhibited increased cytotoxicity compared to CAR-Ms cultured on TCP, and this enhanced functionality persisted throughout in vivo therapy, indicating that the viscoelastic substrate induced mechanical memory in CAR-Ms. Further investigation including mechanical memory reversibility and epigenetic alterations is still needed.

Macrophage possess diverse surface receptors, which can trigger intracellular signaling pathways and alter cellular behavior upon external stimulation[37,64,65]. In this work, we provide innovative insight into the effects of hydrogel priming on CAR-Ms functionality. Our findings reveal that the reduction in cell membrane tension induced by hydrogels, coupled with changes in CAR distribution, leads to the augmentation of downstream signaling. Furthermore, this discovery could have implications for other cells, such as CAR-T cells. In our study, we assessed the cytotoxicity of Gel-CAR-T cells and observed that hydrogels with varying oxidation degree exhibit differing effects. Specifically, hydrogel produced with 20% and 50% oxidized alginate enhanced CAR-T killing efficacy, while hydrogel produced with 95% oxidized alginate resulted in reduced CAR-T killing efficacy (Supplementary Fig. 13A). This phenomenon may be associated with the upregulation of apoptotic factors such as PD1 and CTLA4 (Supplementary Fig. 13B). These findings suggest that hydrogel priming hold promise for enhancing the efficacy of CAR-T therapy and other adoptive cell therapies. However, further research is necessary to determine the optimal hydrogel condition for this purpose. In addition, as CAR undergo distribution changes, classic receptors on macrophage membrane, such as TLR and PRR, may also be affected by hydrogel priming. Once being affected, the functions controlled by these receptors may be impacted as well, which could lead to corresponding cellular behavior change.

In sum, this study introduced a distinct CAR-M therapy treating pulmonary fibrosis. Furthermore, a priming effect by viscoelastic hydrogel on CAR-Ms has been verified with an explained mechanism. Collectively, this study offered valuable perspectives in not only CAR-M therapy development, but also a generalizable method to improve CAR-engineered cell efficacy with high convenience compared to conventional gene editing methods.

Methods

Construction of CAR and lentivirus

Sequences of different anti-FAP scFvs were cloned into a CAR construction, which was on a lentivirus backbone with EF1α as promoter and T2A-EGFRt (truncated EGFR) as label. CAR construction was composed of a CD8 leader sequence, CD8 transmembrane domain and 4-1BB and CD3ζ intracellular domain. A control plasmid containing only EGFRt on the same backbone was also utilized. For membrane imaging of CAR, mCherry was fused to the C-terminal. Lentivirus was packaged in HEK293T cells with infected pMD2.G, pRRE and pRSV-Rev plasmids using Lipo293TM (C0521, Beyotime). After an additional 12 hours of culture, the medium was replaced with fresh culture medium. The supernatant containing the lentivirus particles was collected within 48 hours, and then filtered through a 0.45-μm filter (SLHVR33RB, Millipore). The lentivirus particles were enriched by centrifuging supernatant at 4 °C and 19,500 rpm for 2.5 hours J-26XP, Beckman Colter).

Manufacturing of CAR-Ms

THP-1 and RAW264.7 cells were transduced with lentivirus at an MOI of 5-10 and FACS sorted for high purity. BMDMs were differentiated using L929 cell supernatant for 7 days. On Day 5, BMDMs were transduced with lentivirus at an MOI of 30 and cultured until Day 7. On Day 7, BMDMs were harvested and assessed for CAR expression and function.

Flow cytometry staining and analysis

Cells were harvested and resuspended on ice in flow cytometry buffer. BMDMs were initially treated with Fc block reagent (101319, Biolegend) to prevent non-specific binding, and the Fc block was not washed away. The primary antibody, goat anti-mouse Fab (115-065-072, Jackson), was added and incubated on ice for 1 hour. Afterward, the cells were washed using flow cytometry buffer to remove the primary antibody. The cells were then resuspended in an appropriate volume of flow cytometry buffer and incubated with secondary antibody (405207, Biolegend) for 1 hour on ice, protected from light. Following incubation, the cells were washed again to remove excess secondary antibody. The final pellet was resuspended in flow cytometry buffer and analyzed by flow cytometry (BD LSRFortessa SORP).

Isolation and activation of primary murine lung fibroblasts

Primary lung fibroblasts were isolated from healthy male C57BL/6 mice aged 8–12 weeks. Mice were euthanized, and the lungs were excised and minced on ice. The tissue was digested in 5 ml of enzyme solution prepared in DMDM basal medium containing 0.1% collagenase I (17100017, Gibco), 0.1% collagenase IV (17104019, Gibco), 0.01% hyaluronidase (H8030, Solarbio), and 0.01% DNase I (10104159001, Roche). Samples were incubated at 37 °C for 7 h with gentle shaking every hour to facilitate digestion. Following digestion, residual tissue fragments were dissociated by pipetting, and the suspension was passed through a 40-μm strainer (431750, Corning). Cells were collected by centrifugation at 1000 rpm for 5 min and resuspended in complete DMEM medium. Cells from each lung were seeded into a 10-cm dish and cultured under standard conditions. After 24 h, adherent cells were washed, and fresh medium was added, followed by an additional 24 h of culture. These cells were designated as Day 0. Fibroblast activation was induced by stimulation with 10 ng/ml murine

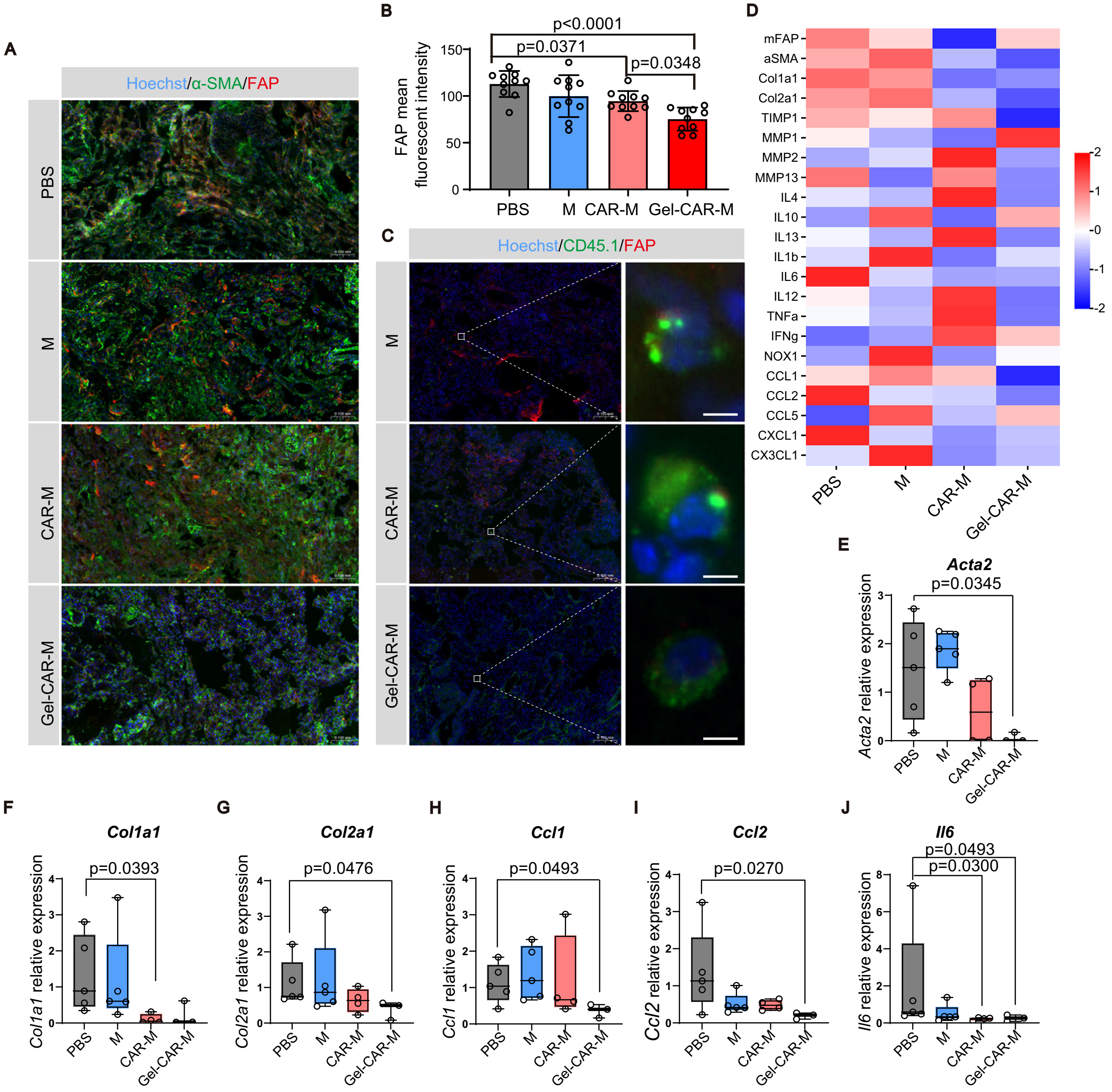

Fig. 5 | Gel-CAR-Ms exhibited advanced efficacy in eradicating FAP-positive cells and restoring the immune microenvironment in fibrotic lungs. **A** Representative image of FAP (Red) immunostaining with α-SMA (Green) of lung and CD45.1 (Green) was used to track injected macrophages. Cell nuclei are labeled with Hoechst (blue). Scale bar was 100 μm. **B** Quantified FAP mean fluorescent intensity. *n* = 10 views from 3–4 mice lungs per treatment. Statistical significance was calculated with one-way ANOVA and is presented as mean ± s.d. **C** Representative image of FAP (Red) immunostaining of lung and CD45.1 (Green) was used to track injected macrophages. Cell nuclei are labeled with Hoechst (blue). The left scale bar was 100 μm, and the right scale bar was 5 μm. **D** Gene expression heat map of average expression values per group. **E**–**J** Relative gene expression of *Acta2*, *Col1a1*, *Col2a1*, *Ccl1*, *Ccl2* and *Il6*. *n* (PBS) = 5, *n* (M) = 5, *n* (CAR-M) = 4, *n* (Gel-CAR-M) = 3 mice in (**D**–**J**). Box-and-whisker plots with the median indicated and Kruskal–Wallis test with Dunn's post-hoc test and FDR correction were used in (**E**–**J**).

TGF-β (763102, Biolegend). Samples were harvested after 1 day and 3 days of stimulation, with medium refreshed once during the 3-day induction period.

FAP Knockdown by shRNA

The shRNA plasmids were purchased from the Biomedical Testing Center at Tsinghua University, with a library (SHPM15, Sigma) containing four shRNA plasmids targeting the mouse FAP protein. The plasmid-containing *E.coli* strains were expanded, followed by plasmid extraction to obtain sufficient plasmids. Lentivirus packaging was then performed according to the described method, and after the lentivirus was produced, it was used to infect wild-type NIH3T3 cells. Puromycin was used for selection, and four shRNA knockdown cell lines were obtained. Samples were taken for WB identification, and the final cell line with FAP protein knockdown was selected for further experiments.

Cytotoxicity assay

NIH3T3 cells were infected with Akaluciferase-T2A-GFP lentivirus, FACS sorted, and then used as targets in a luciferase-based assay. 3T3Aka cells and CAR-Ms were cocultured in a black 96-well plate for 24h, and then the supernatant was discarded, followed by adding TokeOni (808350, FujiFilm) substrate containing medium to measure

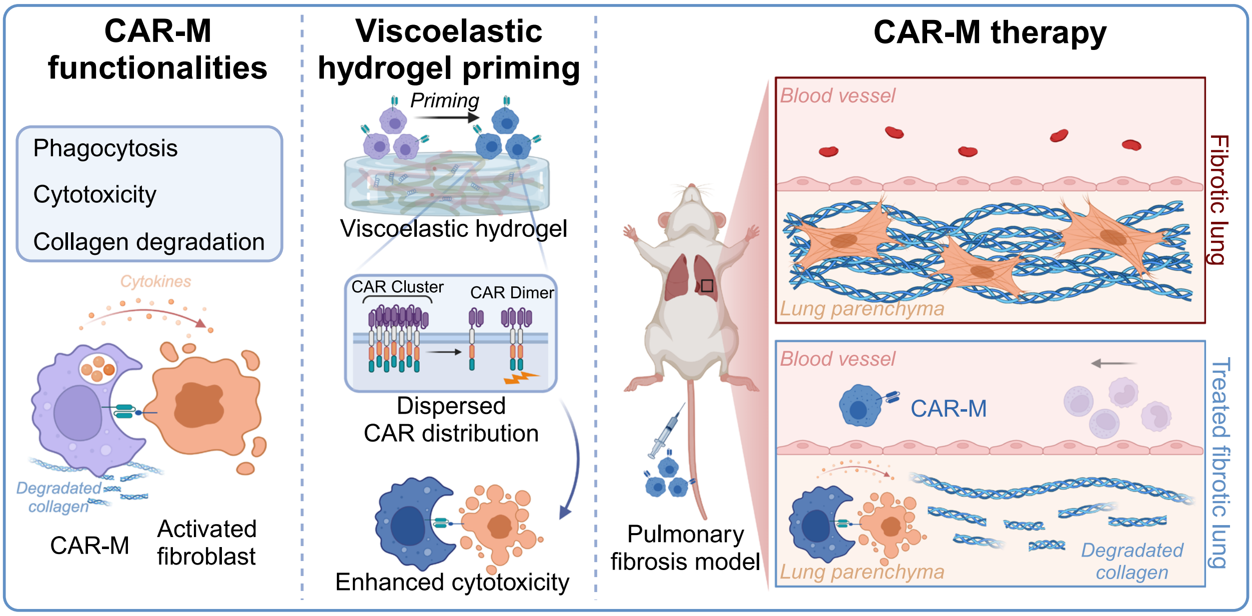

Fig. 6 | Schematic diagram of the constructed CAR-M therapy for pulmonary fibrosis treatment with enhanced therapeutic effect based on viscoelastic hydrogel priming. Macrophages were modified with anti-FAP CAR to activate fibroblasts. The CAR-Ms can treat pulmonary fibrosis not only by phagocytosing and killing activated fibroblasts but also by degrading deposited collagen. Importantly, a viscoelastic hydrogel was utilized to prime CAR-Ms, resulting in dispersed CAR distribution and strengthened cytotoxicity in vitro. Moreover, viscoelastic hydrogel-primed CAR-Ms displayed the strongest therapeutic effect, reversing fibrotic lungs to normal architecture and adjusting the pro-fibrotic immune microenvironment. The figure was created with BioRender. Lab, D. (2025) https://BioRender.com/p06jaon.

the bioluminescence of the remaining live target cells using a microplate reader. For the CAR-Jurkat cell cytotoxicity assay, a CD19-highly-expressing Akaluciferase-labeled Nalm6 cell line was used as the target. CAR-Jurkat cells and Nalm6 cells were co-cultured at an E:T ratio of 2:1 for 24 hours. After co-incubation, cells were collected by centrifugation, resuspended in medium containing luciferase substrate, and bioluminescence was measured using a microplate reader.

$$\text{Killing ratio} = \frac{(\text{3T3Aka signal} - \text{sample signal})}{\text{3T3Aka signal}} \times 100\% \qquad (1)$$

Phagocytosis assay

In order to detect the phagocytosis ability, CAR-Ms and target cells were digested and stained with DeepRed cell tracker (A66433, ThermoFisher) and Green cell tracker (A66434, ThermoFisher), respectively, for 30 minutes at 37 °C. After washing off excess dye with medium, CAR-Ms and target cells were cocultured at 37 °C. For the phagocytosis FACS assay, cells were digested by trypsin (325-043-EL, Wisent) after a 4-hour co-culture, washed, and analyzed by flow cytometry. The percentage of double-positive cells within the macrophage population was used to calculate the phagocytosis ratio. For the time-lapse assay, cells were maintained in a 37 °C live imaging chamber for 8 hours, with images captured every 2 minutes using a Nikon microscope.

Collagen degradation assay

To prepare TAMRA-labeled type I collagen gel, dilute the TAMRA (46406, Thermo Scientific)-collagen (354236, Corning) solution with PBS buffer to a final concentration of 1 mg/mL. Then, add 1 M NaOH solution to adjust the pH of the collagen solution to induce the formation of a collagen hydrogel. Add it to the wells of a plate before hydrogel formation, and place PBS buffer in the adjacent wells to maintain humidity. Incubate the plate at 37 °C for 12 hours to obtain a collagen hydrogel. Seeding co-culture cells on collagen hydrogel for 3 days, then discarding the supernatant and adding collagenase type I to completely degrade the hydrogel. Centrifuge and discard the cell clumps, then add the collagen solution to the wells of a plate. Measure the overall fluorescence of the remaining collagen using a microplate reader (Thermo Scientific Versatile Flash).

Manufacturing of gelatin-alginate hydrogel

Firstly, weigh out 5 g of sodium alginate powder (71238, Sigma) and add it to 15 mL of anhydrous ethanol (E808735, Macklin). To prepare sodium alginate with oxidation degrees of 20%, 50%, and 95%, respectively, weigh 1.0694 g, 2.6735 g, and 5.0797 g of sodium periodate (S817518, Macklin), and dissolve each in 15 mL of deionized water. Protect from light and shake until the sodium alginate is fully dissolved. Heat the sodium alginate powder to 37 °C with magnetic stirring in the dark. Slowly add the sodium periodate solution dropwise and keep stirring the mixture at 37 °C for 6 hours. Add 3 mL of ethylene glycol to terminate the reaction, and continue stirring for 30 minutes. Dialyze the mixture for 3 days. Filter and then lyophilize the oxidized sodium alginate.

Secondly, weigh gelatin and dissolve it in 0.9% sodium chloride solution at 37 °C to prepare a 20% gelatin (73865, Sigma) solution. Filter the solution for sterilization. Dissolve lyophilized sodium alginate in PBS to prepare a 20% oxidized sodium alginate solution. Mix equal volumes of the gelatin solution and oxidized sodium alginate solution thoroughly, then add the mixed solution to a well plate and place it in a 37 °C environment for 24 hours. After that, add 0.1 M calcium chloride (C915443, Macklin) solution on top of the gel for 3 hours.

Preparation of hydrogel primed CAR-Ms

Prior to use, pre-fabricated hydrogels were washed three times with sterile PBS, then incubated with an appropriate volume of complete macrophage culture medium to fully cover the hydrogel surface. The hydrogels were soaked at 37 °C in a humidified incubator for 24 hours to allow equilibration. After incubation, the hydrogels were washed again with PBS three times to remove residual medium. CAR-Ms

(1×10^6 cells) were resuspended in 2.5 mL of fresh culture medium and gently dispensed onto the hydrogel surface. The plates were left undisturbed for 5 minutes to allow cells to settle and adhere, and then transferred to a 37 °C incubator for further culture. After 24 hours of incubation, the plates were carefully removed from the incubator, and the supernatant was aspirated to expose the hydrogel surface. For RAW264.7 cells, 500 µL of fresh culture medium was gently pipetted onto the hydrogel surface to dislodge the adherent cells by gentle flushing. The resulting cell suspension was collected and centrifuged, and the cell pellet was resuspended in fresh culture medium for downstream applications. For BMDMs, the hydrogel surface was covered with a digestion solution containing 1 mg/mL type I collagenase prepared in DMEM basal medium. The samples were incubated at 37 °C for 5 minutes to facilitate cell detachment, followed by flushing with culture medium to release the cells. Cell culture conditions were maintained under endotoxin-free conditions (Supplementary Table 1). Cells were centrifuged at 1000 rpm for 5 minutes, washed three times with PBS to remove residual hydrogel debris, and then resuspended in fresh medium for subsequent use.

Cell membrane tension measurement

Prepare serum-free DMEM medium and add Flipper TR fluorescent probe (HY-D2316, Cytoskeleton) at a concentration of 1 µM. Resuspend cells in probe-containing medium and incubate the cells at 37 °C for at least 30 minutes, protect from light, and bring to the FLIM microscope (FV1200 Confocal, Olymplus). Use 488 nm excitation light to excite the fluorescent probe and detect emission with a 600 nm filter. Measure cell membrane tension using the membrane tension analysis module in the microscope.

Membrane protein imaging and single-molecule photobleaching

CAR-Ms were primed on hydrogels for 24 hours. The CAR was conjugated with mCherry protein. After priming, the cells were collected and fixed with 4% paraformaldehyde. Following fixation, the cells were washed with PBS. Membrane CAR-mCherry fluorescent imaging was performed using a TIRF microscope (Nikon N-SIM E super-resolution microscope) with a ×100 objective lens. The number of membrane CAR-mCherry clusters in the images was counted for further analysis. For single-molecule photobleaching, fixed cells underwent fluorescence photobleaching, with continuous imaging captured at a frequency of 50 ms per frame. The acquired images were processed using deconvolution. Regions of interest were delineated, and fluorescence intensity curves for each fluorescent spot were extracted. The number of photobleaching steps was then counted based on the intensity changes in the fluorescence curves.

Quantitative real-time PCR

RNA was first extracted from the samples using Trizol solution (R401, Vazyme), and cells were gently homogenized with a pipette. Chloroform (C112044, Aladdin) was then added to separate the RNA into the aqueous phase. Equal volumes of isopropanol (I112010, Aladdin) were added to precipitate the RNA, which was then dissolved in RNase-free water, and its concentration was measured on a Nanodrop (NanoDrop One, Thermo Fisher Scientific). Next, RNA was reverse transcribed into cDNA. The qPCR reaction mixture was prepared in a total volume of 10 µL, including 20 ng of cDNA, 5 µL of 2× SYBR Mix (R211, Vazyme), and forward and reverse primers at a final concentration of 0.5 nM. The remaining volume was adjusted with RNase-free water. GAPDH was used as the internal control, and relative gene expression was analyzed using the Ct ($2^{-\Delta\Delta Ct}$) method.

Immunofluorescence staining

Cells or tissue cryosections were fixed with 4% PFA (P1110, Solarbio) for 15 minutes and washed three times with PBS. Blocking and permeabilization were performed with 5% BSA (fetal bovine serum) and 0.5% Triton X-100 (T109027, Aladdin) in PBS at room temperature for 1 hour. The primary antibody (Biotin-SP-AffiniPure Goat Anti-Mouse IgG, F(ab')[2], 115-065-072, Jackson; anti-FAP, ab53066, Abcam; anti-α-SMA, MA5-11547, Invitrogen; anti-p-SYK, 2710 T, Cell Signaling Technology; anti-p-ERK1/2, 4377S, Cell Signaling Technology; anti-p-JNK, 1255S, Cell Signaling Technology) was diluted in 1% BSA solution and incubated overnight at 4 °C. After incubation, samples were brought to room temperature and washed three times with PBS. The secondary antibody, diluted in 5% BSA solution, was added, and samples were incubated at room temperature, protected from light, for 1 hour. The secondary antibody solution was then discarded, and Hoechst (C1022, Beyotime) staining solution was applied for nuclear staining, incubating for 15 minutes at room temperature, protected from light. After discarding the staining solution, the samples were washed three times with PBS. Finally, coverslips were mounted using an anti-fade mounting medium (P1023, Beyotime). Images were captured using the Axio Scan.Z1 Zeiss automated digital slide scanner.

Immunohistochemistry staining

Paraffin-embedded tissue sections were mounted on slides and subjected to a dewaxing procedure. The sections were immersed in xylene for 7 minutes, repeated three times, followed by a series of alcohol washes: 100%, 95%, 90%, 80%, and 70% ethanol, each for 5 minutes. The sections were then washed in deionized water for 5 minutes, repeated twice. Next, the sections were incubated in sodium citrate solution (C1032, Solarbio) for antigen retrieval, placed in the solution, and microwaved at high power for 10 minutes. After cooling to room temperature, the slides were washed three times with PBS buffer. The sections were then incubated with 3% hydrogen peroxide to block endogenous peroxidase activity for 10 minutes, protected from light. Afterward, the slides were washed three times with PBS buffer, and then blocked with 5% BSA (A8020, Solarbio) solution at room temperature for 30 minutes. The BSA solution was discarded, and the primary antibody, diluted in 5% BSA solution, was applied and incubated overnight at 4 °C in a humid chamber. After incubation with the primary antibody, the slides were brought to room temperature and washed three times with PBS buffer. A horseradish peroxidase-conjugated anti-mouse IgG polymer was added, and the slides were incubated at room temperature for 1 hour. The slides were then washed three times with PBS buffer (SP0023, Bioss). The sections were developed using DAB solution for 30 minutes, and the reaction was stopped by washing with deionized water (DA1010, Solarbio). Hematoxylin (ZLI-9610, Zhongshan Jinqiao) was applied for nuclear staining for 10 seconds, followed by rinsing in running water to blue the sections. Finally, the slides were dehydrated by sequential immersion in 70%, 80%, 90%, 95%, and 100% ethanol, each for 5 minutes, followed by immersion in xylene for 7 minutes, repeated three times. The sections were then mounted with neutral resin (G8590, Solarbio) for final sealing.

Reducing and non-reducing western blot

First, cell samples were collected, with each sample containing at least two million cells. The cells were washed once with PBS, centrifuged, and the cell pellets were stored at −80 °C. For non-reducing samples, gentle lysis buffer (Leagene, PS0009) was added, along with 100× PMSF (ST506, Beyotime) and 100× protease inhibitor (P1005, Beyotime), and mixed by pipetting. The cells were lysed on ice for 10 minutes and then sonicated at 40 W power for 2 cycles of 6 seconds each, followed by centrifugation at 12,000 × *g* for 10 minutes at 4 °C. The supernatant was taken to measure protein concentration. The remaining supernatant was mixed with 5× non-reducing loading buffer (Biosharp, BL511B) and heated at 37 °C for 30 minutes.

For reducing samples, strong lysis buffer (Leagene, PS0013) was used, along with 100× PMSF and 100× protease inhibitor, and mixed by pipetting. The cells were lysed on ice for 10 minutes, followed by sonication at 40 W power for three cycles of 6 seconds each. The samples were then centrifuged at 12,000 × *g* for 10 minutes at 4 °C. The supernatant was used to measure protein concentration, and the remaining supernatant was mixed with 5× reducing loading buffer (P0286, Beyotime) and heated at 100 °C for 10 minutes.

Protein concentrations in different samples were measured using the BCA protein assay kit (P0009, Beyotime). 20 µg of protein was loaded for each sample, along with a protein ladder (MF212, Mei5bio). The gel was run at 80 V for 30 minutes, followed by 120 V for 1.5 hours. To transfer the proteins, a transfer sandwich was assembled using PVDF membrane (IPVH00010, Merck Millipore), and the transfer was performed at 350 mA for 2 hours. After the transfer, the PVDF membrane was removed and blocked with 5% non-fat milk for 1 hour at room temperature. The membrane was then incubated with the primary antibody solution overnight at 4 °C. After incubation, the membrane was washed three times with TBST buffer (T1087, Solarbio). Next, the membrane was incubated with the secondary antibody solution at room temperature for 1 hour. Afterward, the membrane was washed three times with TBST buffer and exposed using ECL (enhanced chemiluminescence) substrate (MF074-05, Mei5bio).

Establishment of a pulmonary fibrosis model and cell injection

Pulmonary fibrosis was induced in 10-week-old male C57BL/6 mice using a bleomycin (S1214, Selleck) solution prepared in PBS at a concentration of 5 mg/mL. After weighing the mice, anesthesia was administered via intraperitoneal injection of Avertin. Using a flat-tip microsyringe, the appropriate volume of bleomycin solution was drawn based on a dosage of 1 µL/g body weight. A laryngoscope was used to illuminate the tracheal opening. The syringe needle was then inserted into the trachea, and bleomycin was slowly injected. After injection, the mouse was positioned with its head upward on an incline to facilitate recovery. Mice were monitored for weight and general condition every three days post-injection. All animal protocols used in this study were approved by the Institutional Animal Care and Use Committee of Tsinghua University. On Day −1 (one day before bleomycin induction), bone marrow cells were harvested from mice and differentiated into primary macrophages using L929-conditioned medium, as previously described. On Day 4 after bleomycin administration, the primary macrophages were transduced with lentivirus to generate CAR-Ms. On Day 6, CAR-Ms were collected and cultured on a viscoelastic hydrogel. On Day 7, hydrogel-primed CAR-Ms were resuspended in PBS, and 1×10^6 cells in 200 µL were administered via tail vein injection per mouse. A second intravenous injection of the same cell dose was performed on Day 14.

RNA bulk sequencing

Bulk RNA-seq library preparation, sequencing and analysis were performed by GENEWIZ (Suzhou, China). The company followed its standardized operating procedures, including total RNA extraction, quality assessment, library construction, and Illumina sequencing. Raw sequencing reads were processed using Cutadapt (v1.9.1) to remove adapters and low-quality bases. Gene-level counts were obtained using HTSeq (v0.6.1) from uniquely mapped exon-overlapping reads. Downstream analyses were performed in R. Differential gene expression analysis was conducted using DESeq2 (v1.34.0), applying median-of-ratios normalization, dispersion estimation, Wald testing, and Benjamini–Hochberg correction. Genes with adjusted $P < 0.05$ were considered differentially expressed. Data visualization, including volcano plots and heatmaps, was performed using ggplot2 and pheatmap. All sequencing data are available at the Sequence Read Archive database via the accession number PRJNA1355556.

Statistical analysis

Statistical analyses in this study were conducted using GraphPad Prism 6.0 software. Data are presented as mean ± standard deviation (SD). We used the Anderson-Darling, D'Agostino-Pearson, Shapiro–Wilk, and Kolmogorov–Smirnov tests to assess the normality of sample data. For significance testing between two groups, if the data were normally distributed, we applied *t* test; if not, we used the Mann–Whitney test. For multiple group comparisons, normally distributed data were analyzed using one-way ANOVA with Tukey's post hoc test, while non-normally distributed data were analyzed using the Kruskal–Wallis test. Exact *P* values are indicated in the figures, with $P < 0.05$ considered statistically significant.

Ethical statement

All animal protocols, including mouse housing, induction of pulmonary fibrosis, and cell therapy administration, were approved by the Institutional Animal Care and Use Committee of Tsinghua University.

Reporting summary

Further information on research design is available in the Nature Portfolio Reporting Summary linked to this article.

Data availability

The main data supporting the results in this study are available within the paper and its Supplementary Information. The raw RNA-seq data are available at the Sequence Read Archive database via the accession number PRJNA1355556. Source data are provided with this paper.

References

1. Hirayama, D., Iida, T. & Nakase, H. The phagocytic function of macrophage-enforcing innate immunity and tissue homeostasis. *Int. J. Mol. Sci.* **19**, 92 (2017).
2. Chen, S. et al. Macrophages in immunoregulation and therapeutics. *Sig. Transduct. Target Ther.* **8**, 1–35 (2023).
3. Klichinsky, M. et al. Human chimeric antigen receptor macrophages for cancer immunotherapy. *Nat. Biotechnol.* **38**, 947–953 (2020).
4. Zhang, J. et al. Generation of anti-GD2 CAR macrophages from human pluripotent stem cells for cancer immunotherapies. *Stem Cell Rep.* **18**, 585–596 (2023).
5. Lu, J. et al. CAR Macrophages: a promising novel immunotherapy for solid tumors and beyond. *Biomark. Res.* **12**, 86 (2024).
6. Hadiloo, K., Taremi, S., Heidari, M. & Esmaeilzadeh, A. The CAR macrophage cells, a novel generation of chimeric antigen-based approach against solid tumors. *Biomark. Res.* **11**, 103 (2023).
7. Dai, H. et al. Chimeric antigen receptor-modified macrophages ameliorate liver fibrosis in preclinical models. *J. Hepatol.* **80**, 913–927 (2024)
8. Kisseleva, T. & Brenner, D. A. Fibrogenesis of parenchymal organs. *Proc. Am. Thorac. Soc.* **5**, 338–342 (2008).
9. Taskar, V. S. & Coultas, D. B. Is idiopathic pulmonary fibrosis an environmental disease?. *Proc. Am. Thorac. Soc.* **3**, 293–298 (2006).
10. Richeldi, L., Collard, H. R. & Jones, M. G. Idiopathic pulmonary fibrosis. *Lancet* **389**, 1941–1952 (2017).
11. Ley, B. & Collard, H. R. Epidemiology of idiopathic pulmonary fibrosis. *Clin. Epidemiol.* **5**, 483–492 (2013).
12. Sgalla, G., Biffi, A. & Richeldi, L. Idiopathic pulmonary fibrosis: diagnosis, epidemiology and natural history. *Respirology* **21**, 427–437 (2016).
13. Sauleda, J., Núñez, B., Sala, E. & Soriano, J. B. Idiopathic pulmonary fibrosis: epidemiology, natural history, phenotypes. *Med Sci.* **6**, 110 (2018).
14. Martinez, F. J. et al. Idiopathic pulmonary fibrosis. *Nat. Rev. Dis. Prim.* **3**, 1–19 (2017).
15. White, M. J. V. et al. Blocking antibodies against integrin-α3, -αM, and -αMβ2 de-differentiate myofibroblasts, and improve lung fibrosis and kidney fibrosis. *Sci. Rep.* **14**, 21623 (2024).
16. Yang, A.-T. et al. Fibroblast activation protein activates macrophages and promotes parenchymal liver inflammation and fibrosis. *Cell Mol. Gastroenterol. Hepatol.* **15**, 841–867 (2022).

17. Lavis, P., Garabet, A., Cardozo, A. K. & Bondue, B. The fibroblast activation protein alpha as a biomarker of pulmonary fibrosis. *Front. Med*. **11**, 1393778 (2024).
18. Lei, A. et al. A second-generation M1-polarized CAR macrophage with antitumor efficacy. *Nat. Immunol*. **25**, 102–116 (2024).
19. Wang, X. et al. Metabolic reprogramming via ACOD1 depletion enhances function of human induced pluripotent stem cell-derived CAR-macrophages in solid tumors. *Nat. Commun*. **14**, 5778 (2023).
20. Tang, C. et al. mRNA-laden lipid-nanoparticle-enabled in situ CAR-macrophage engineering for the eradication of multidrug-resistant bacteria in a sepsis mouse model. *ACS Nano* **18**, 2261–2278 (2024).
21. Liu, M. et al. CAR-macrophages and CAR-T cells synergistically kill tumor cells in vitro. *Cells* **11**, 3692 (2022).
22. Murray, P. J. Macrophage polarization. *Annu. Rev. Physiol*. **79**, 541–566 (2017).
23. Das, A. et al. Monocyte and macrophage plasticity in tissue repair and regeneration. *Am. J. Pathol*. **185**, 2596–2606 (2015).
24. Sridharan, R., Cavanagh, B., Cameron, A. R., Kelly, D. J. & O'Brien, F. J. Material stiffness influences the polarization state, function and migration mode of macrophages. *Acta Biomater*. **89**, 47–59 (2019).
25. Chen, M. et al. Substrate stiffness modulates bone marrow-derived macrophage polarization through NF-κB signaling pathway. *Bioact. Mater*. **5**, 880–890 (2020).
26. Trappmann, B. et al. Extracellular-matrix tethering regulates stem-cell fate. *Nat. Mater*. **11**, 642–649 (2012).
27. Tetrick, M. G. & Murphy, C. J. Leveraging tunable nanoparticle surface functionalization to alter cellular migration. *ACS Nanosci. Au* **4**, 205–215 (2024).
28. Jiang, S. et al. Cryoprotectant enables structural control of porous scaffolds for exploration of cellular mechano-responsiveness in 3D. *Nat. Commun*. **10**, 3491 (2019).
29. Kalashnikov, N. & Moraes, C. Substrate viscoelasticity affects human macrophage morphology and phagocytosis. *Soft Matter* **19**, 2438–2445 (2023).
30. Zhou, Y.-W. & Wu, Y. Substrate viscoelasticity amplifies distinctions between transient and persistent LPS-induced signals. *Adv. Health Mater*. **11**, e2102271 (2022).
31. Hossain, M. Z. & Stroberg, W. Bilayer tension-induced clustering of the UPR sensor IRE1. *Biochim. Biophys. Acta Biomembr*. **1866**, 184262 (2024).
32. Xie, P. et al. Membrane proteins and membrane curvature: mutual interactions and a perspective on disease treatments. *Biomolecules* **13**, 1772 (2023).
33. Shi, Z. & Baumgart, T. Membrane tension and peripheral protein density mediate membrane shape transitions. *Nat. Commun*. **6**, 5974 (2015).
34. Lachowski, D. et al. Substrate stiffness-driven membrane tension modulates vesicular trafficking via caveolin-1. *ACS Nano* **16**, 4322–4337 (2022).
35. Fournier, J.-B. Membrane protein clustering from tension and multibody interactions. *EPL* **146**, 57001 (2024).
36. Beedle, A. E., Williams, A., Relat-Goberna, J. & Garcia-Manyes, S. Mechanobiology — chemical origin of membrane mechanical resistance and force-dependent signaling. *Curr. Opin. Chem. Biol*. **29**, 87–93 (2015).
37. Li, M., Xing, X., Yuan, J. & Zeng, Z. Research progress on the regulatory role of cell membrane surface tension in cell behavior. *Heliyon* **10**, e29923 (2024).
38. Wang, L.-C. S. et al. Targeting fibroblast activation protein in tumor stroma with chimeric antigen receptor T cells can inhibit tumor growth and augment host immunity without severe toxicity. *Cancer Immunol. Res*. **2**, 154–166 (2014).
39. Tran, E. et al. Immune targeting of fibroblast activation protein triggers recognition of multipotent bone marrow stromal cells and cachexia. *J. Exp. Med* **210**, 1125–1135 (2013).
40. Brocks, B. et al. Species-crossreactive scFv against the tumor stroma marker "fibroblast activation protein" selected by phage display from an immunized FAP−/− knock-out mouse. *Mol. Med*. **7**, 461–469 (2001).
41. Leyva, F. J., Anzinger, J. J., McCoy, J. P. & Kruth, H. S. Evaluation of transduction efficiency in macrophage colony-stimulating factor differentiated human macrophages using HIV-1 based lentiviral vectors. *BMC Biotechnol*. **11**, 13 (2011).
42. Burke, B., Sumner, S., Maitland, N. & Lewis, C. E. Macrophages in gene therapy: cellular delivery vehicles and in vivo targets. *J. Leukoc. Biol*. **72**, 417–428 (2002).
43. Distler, T. et al. Ionically and enzymatically dual cross-linked oxidized alginate gelatin hydrogels with tunable stiffness and degradation behavior for tissue engineering. *ACS Biomater. Sci. Eng*. **6**, 3899–3914 (2020).
44. Abasalizadeh, F. et al. Alginate-based hydrogels as drug delivery vehicles in cancer treatment and their applications in wound dressing and 3D bioprinting. *J. Biol. Eng*. **14**, 8 (2020).
45. Sprenger, L. et al. Composite alginate dialdehyde-gelatin (ADA-GEL) hydrogel containing short ribbon-shaped fillers for skeletal muscle tissue biofabrication. *ACS Appl. Mater. Interfaces* **16**, 44605–44622 (2024).
46. Page-McCaw, A., Ewald, A. J. & Werb, Z. Matrix metalloproteinases and the regulation of tissue remodelling. *Nat. Rev. Mol. Cell Biol*. **8**, 221–233 (2007).
47. Ozga, A. J., Chow, M. T. & Luster, A. D. Chemokines and the immune response to cancer. *Immunity* **54**, 859 (2021).
48. Hu, J. et al. Cell membrane patches transfer CAR molecules from a cellular depot to conventional T cells for constructing innovative fused-CAR-T cells without necessitating genetic modification. *Exp. Hematol. Oncol*. **13**, 75 (2024).
49. Kouro, T., Himuro, H. & Sasada, T. Exhaustion of CAR T cells: potential causes and solutions. *J. Transl. Med*. **20**, 239 (2022).
50. Ni, Y. et al. Macrophages modulate stiffness-related foreign body responses through plasma membrane deformation. *Proc. Natl. Acad. Sci*. **120**, e2213837120 (2023).
51. Pandzic, E., Whan, R. & Macmillan, A. Rapid FLIM measurement of membrane tension probe flipper-TR. In *Membrane Lipids: Methods and Protocols* (ed. Cranfield, C. G.) 257–283 (Springer US, New York, NY, 2022). https://doi.org/10.1007/978-1-0716-1843-1_20.
52. Ruan, H. et al. N-(3-oxododecanoyl) homoserine lactone is a generalizable plasma membrane lipid-ordered domain modifier. *Front. Physiol*. **12**, 758458 (2022).
53. Zhang, W. et al. Chimeric antigen receptor macrophage therapy for breast tumours mediated by targeting the tumour extracellular matrix. *Br. J. Cancer* **121**, 837–845 (2019).
54. Gialeli, C. et al. PDGF/PDGFR signaling and targeting in cancer growth and progression: focus on tumor microenvironment and cancer-associated fibroblasts. *Curr. Pharm. Des*. **20**, 2843–2848 (2014).
55. Díaz-Lezama, N. et al. PDGF receptor alpha signaling is key for müller cell homeostasis functions. *Int. J. Mol. Sci*. **22**, 1174 (2021).
56. Klinkhammer, B. M., Floege, J. & Boor, P. PDGF in organ fibrosis. *Mol. Asp. Med*. **62**, 44–62 (2018).
57. Xiao, W. et al. Chimeric antigen receptor-modified T-cell therapy for platelet-derived growth factor receptor α-positive rhabdomyosarcoma. *Cancer* **126**, 2093–2100 (2020).
58. Cho, J. H. et al. Engineering advanced logic and distributed computing in human CAR immune cells. *Nat. Commun*. **12**, 792 (2021).
59. Zah, E. et al. Systematically optimized BCMA/CS1 bispecific CAR-T cells robustly control heterogeneous multiple myeloma. *Nat. Commun*. **11**, 2283 (2020).

60. Yang, C., Tibbitt, M. W., Basta, L. & Anseth, K. S. Mechanical memory and dosing influence stem cell fate. *Nat. Mater.* **13**, 645–652 (2014).
61. Dudaryeva, O. Y., Bernhard, S., Tibbitt, M. W. & Labouesse, C. Implications of cellular mechanical memory in bioengineering. *ACS Biomater. Sci. Eng.* **9**, 5985–5998 (2023).
62. Na, J. et al. Mechanical memory based on chromatin and metabolism remodeling promotes proliferation and smooth muscle differentiation in mesenchymal stem cells. *FASEB J.* **38**, e23538 (2024).
63. Scott, A. K. et al. Mechanical memory stored through epigenetic remodeling reduces cell therapeutic potential. *Biophys. J.* **122**, 1428–1444 (2023).
64. Kreysing, E. et al. Effective cell membrane tension is independent of polyacrylamide substrate stiffness. *PNAS Nexus* **2**, pgac299 (2023).
65. Sitarska, E. & Diz-Muñoz, A. Pay attention to membrane tension: mechanobiology of the cell surface. *Curr. Opin. Cell Biol.* **66**, 11–18 (2020).

Acknowledgements

We thank Dr. Hui Zhao and Dr. Yinqiang Sui for their generous contribution of anti-CD19 CAR sequences, Nalm6 cells and their assistance in constructing the CD69 upregulation assay in this study. We appreciate Dr. Liping Deng for her guidance and suggestions in plasmid construction. We also thank Xin Wang for her help in establishing a single-molecular photobleaching assay. Some of the illustrations were created with Biorender.com. This work was supported by the National Natural Science Foundation of China-82125018 (Y.D.), National Natural Science Foundation of China-32430058 (Y.D.), and Natural Science Foundation of Beijing, China-Z230016 (Y.D.). Schematics were created using several icon elements from BioRender.com.

Author contributions

Y.Z. and Y.D. conceived the study. Z.L. established the hydrogel preparation method and assisted in viscoelasticity measurements. Y.Z. performed cell engineering, phagocytosis and cytotoxicity assays, hydrogel priming of cells, and establishment and treatment of the mouse pulmonary fibrosis model. Z.L. assisted with hydrogel-related experiments. Y.A. performed tail vein injections. R.Z. contributed to pulmonary fibrosis modeling and tail vein injections. W.K. assisted with data analysis and generated 3D images of fibrotic lungs. Y.D. supervised the project. Y.Z. wrote the original draft. Y.Z. and Y.D. reviewed and edited the manuscript.

Competing interests

The authors declare no competing interests.

Additional information

Supplementary information The online version contains supplementary material available at https://doi.org/10.1038/s41467-025-68033-4.

Correspondence and requests for materials should be addressed to Yanan Du.

Peer review information *Nature Communications* thanks Hua Wang, and the other, anonymous, reviewer(s) for their contribution to the peer review of this work. A peer review file is available.

Reprints and permissions information is available at http://www.nature.com/reprints